

Full polarization study of SiO masers at 86 GHz

Fabrice Herpin, Alain Baudry, Clemens Thum, Dave Morris, Helmut Wiesemeyer

▶ **To cite this version:**

Fabrice Herpin, Alain Baudry, Clemens Thum, Dave Morris, Helmut Wiesemeyer. Full polarization study of SiO masers at 86 GHz. Astronomy and Astrophysics - A&A, 2006, 450-2, pp.667-680. 10.1051/0004-6361:20054255 . hal-00016435

HAL Id: hal-00016435
https://hal.science/hal-00016435

Submitted on 5 Jan 2006

HAL is a multi-disciplinary open access archive for the deposit and dissemination of scientific research documents, whether they are published or not. The documents may come from teaching and research institutions in France or abroad, or from public or private research centers.

L'archive ouverte pluridisciplinaire **HAL**, est destinée au dépôt et à la diffusion de documents scientifiques de niveau recherche, publiés ou non, émanant des établissements d'enseignement et de recherche français ou étrangers, des laboratoires publics ou privés.

Astronomy & Astrophysics manuscript no. polar˙v˙nov.hyper6809 January 5, 2006
(DOI: will be inserted by hand later)

Full polarization study of SiO masers at 86 GHz

F. Herpin[1], A. Baudry[1], C. Thum[2], D. Morris[2,3] and H. Wiesemeyer[2]

[1] Observatoire Aquitain des Sciences de l'Univers, Laboratoire d'Astrodynamique, d'Astrophysique et d'Aéronomie de Bordeaux, CNRS/INSU UMR n° 5804, BP 89, 33270, France
[2] IRAM, 300 rue de la Piscine, Domaine Universitaire, 38406 Saint Martin d'Hères, France
[3] Present address: Raman Research Institute, 560080 Bangalore, India

the date of receipt and acceptance should be inserted later

Abstract. We study the polarization of the SiO maser emission in a representative sample of evolved stars in order to derive an estimate of the strength of the magnetic field, and thus determine the influence of this magnetic field on evolved stars. We made simultaneous spectroscopic measurements of the 4 Stokes parameters, from which we derived the circular and linear polarization levels. The observations were made with the IF polarimeter installed at the IRAM 30m telescope. A discussion of the existing SiO maser models is developed in the light of our observations. Under the Zeeman splitting hypothesis, we derive an estimate of the strength of the magnetic field. The averaged magnetic field varies between 0 and 20 Gauss, with a mean value of 3.5 Gauss, and follows a $1/r$ law throughout the circumstellar envelope. As a consequence, the magnetic field may play the role of a shaping, or perhaps collimating agent of the circumstellar envelopes in evolved objects.

ccsd-00016435, version 1 - 5 Jan 2006

Keywords. Maser: SiO – polarization– survey – stars: late-type, evolution, magnetic field

1. Introduction

The prodigious mass loss observed in numerous and widespread evolved stars make these objects the main recycling agents of the interstellar medium, and thus one of the most important objects in the Universe. Even though our knowledge of evolved stars has considerably improved over recent years, some of their main characteristics remain insufficiently understood (see the review by Herwig 2003): which mechanisms are responsible for their drastic change of geometry when evolving to the Planetary Nebula (hereafter PN) stage ? What is powering so efficiently the mass loss and could the magnetic field play a major role ?

Important information about the physics and chemistry prevailing in the circumstellar envelope (hereafter *CSE*) of evolved stars can be retrieved from radiowave line emission of molecules, specially from maser emission (see the review by Bujarrabal 2003). These envelopes can be probed at different depths through the study of three masing molecules, OH, H_2O and SiO. Our current knowledge indicates that:

- OH radiation traces the outer part of the envelope, at 1000-10000 AU from the central star;
- H_2O molecules are located at intermediate distances, i.e. a few 100 AU;
- SiO maser emission comes from the inner regions of the envelope, between 5 to 10 AU (a few stellar radii $R_\star$).

The SiO maser emission is produced in small gas cells, and is known to be polarized. The polarization (circular or linear) and angle of the emission can be measured and thus improve our knowledge of these objects. In addition, studying the maser polarization can shed light on the maser theory itself. As explained further in this paper, several uncertainties in the theory make data interpretation often difficult, and new observational data are helpful. One of the most interesting quantities that can be derived from polarization measurements is the stellar magnetic field. According to theory (e.g. Elitzur 1996 or 2002), measurement of the maser radiation polarization can lead to an estimation of the magnetic field strength B and can reveal its spatial structure (via interferometric observations). In single dish observations, all of the maser components get smeared within the beam and only the mean value of B along the line of sight ($B_{//}$) can be derived. Only SiO masers are capable of tracing the magnetic field as close as ~ 5 AU from the central star. But if SiO masers are to be used as a B-field tracer, we first need to give evidence that SiO masers are reliable B-field tracers. This requires more detailed theories than available today. Nevertheless, we tentatively derive in this work the field strength in the CSE inner layers of several evolved stars.

Research on astronomical masers polarization is very active but is made difficult both by the lack of specific instrumental facilities and by the excitation and propagation of the masers themselves. Until now, numerous polarimetric observations of OH masers have been done, several of H_2O masers, but few of SiO maser emission. Few SiO polarimetric observations have been done with VLBI giving the very first images of the magnetic field in some objects (e.g. Kemball & Diamond 1997 in TX Cam). Most of the early SiO studies were done

in linear polarization. The first complete SiO polarimetric observations were performed by Johnson & Clark (1975), then by Troland et al. (1979); emission was found to be typically 15-30 % linearly polarized and to exhibit no circular polarization. Barvainis, McIntosh & Predmore (1987), and McIntosh et al. (1989) measured circular polarization of 1 – 9 % in several stars. Circular (0-4 %) and linear (3.7-9.7 %) polarizations were measured in VY CMa by McIntosh, Predmore & Patel (1994). Later, Kemball & Diamond (1997) made the first image of the magnetic field in the atmosphere of TX Cam, measuring a circular polarization level of 5 % with some features showing polarization up to 30-40 %.

It must be stressed that SiO, as H_2O, is a non-paramagnetic species. Zeeman splitting exists but the sublevels overlap; the effect is thus undetectable and hence only net polarization can be used to trace the magnetic field. The current status of our knowledge on the magnetic field strength can be summarized as follows:

- between 1000-10000 AU, $B_{//} \sim 5 - 20$ mG (OH masers, e.g. Kemball & Diamond 1997, Szymczak & Cohen 1997);
- at a few 100 AU from the star, $B_{//} \sim$ a few 100 mG (H_2O masers, e.g. Vlemmings, Diamond & van Langevelde 2001, Vlemmings, van Langevelde & Diamond 2005);
- at 5-10 AU, $B_{//} \sim 5 - 10$ G (SiO masers; Kemball & Diamond 1997, in TX Cam).

The main purpose of this work is to measure and analyze the SiO maser polarization in terms of magnetic field strength in a representative sample of evolved stars. Our observations are presented in Section 2; they include simultaneous spectroscopic measurements of the 4 Stokes parameters. The results for individual stars are discussed in Section 3. In Section 4, we compare our data with predictions from existing SiO maser models and initiate a discussion on the validity of these models. Within the limitations of one of these models we derive the magnetic field strength and try to determine the role of the magnetic field. More broadly, a summary of the magnetic field topic in evolved stars is also given in Section 4. In Section 5 we give some concluding remarks.

2. Observations

An electromagnetic plane wave is defined by two components (horizontal and vertical):

$$e_H(z,t) = E_H\, e^{j(\omega t - kz - \delta)} \quad (1)$$

$$e_V(z,t) = E_V\, e^{j(\omega t - kz)} \quad (2)$$

where δ is the phase difference between horizontal and vertical components.

Its energy flux is described by the 4 Stokes parameters:

$$I = < {E_H}^2 > + < {E_V}^2 > \quad (3)$$

$$Q = < {E_H}^2 > - < {E_V}^2 > \quad (4)$$

$$U = 2 < E_H E_V cos\, \delta > \quad (5)$$

$$V = 2 < E_H E_V sin\, \delta > \quad (6)$$

From these parameters, one deduces:

- the circular polarization rate $p_C = V/I$
- the linear polarization rate $p_L = \sqrt{Q^2 + U^2}/I$
- the polarization angle $\chi = \frac{\arctan(U/Q)}{2}$

The linear/circular polarization rate is sometimes called the linear/circular fractional polarization.

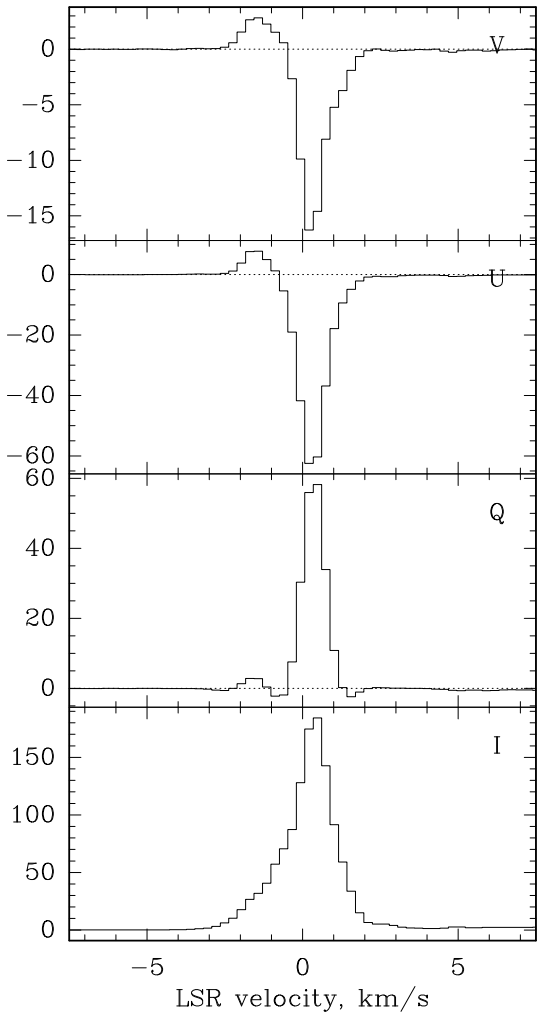


Fig. 1. V, U, Q and I Stokes parameters for R Leo. I, V, U and Q are given in Kelvins ($Ta^\star$; the conversion factor is 6 Jy/K).

We present here spectroscopic measurements of the 4 Stokes parameters (see Fig. 1). The observations were made with the IF polarimeter installed at the IRAM 30m telescope on Pico Veleta, Spain (Thum et al. 2003). Simultaneous measurements of I, U, Q, V allow us to calculate I, p_L, p_C and χ for each velocity channel. The polarization angle calibration (i.e. the sign of Stokes U) was verified by observations of the Crab Nebula. Moreover, planets (polarization of planets is negligible at our frequency) have been used to check the instrumental polarization on the optical axis.

The instrumental beam polarization is known to be stronger in Stokes Q and U than in Stokes V (known to be $\leq$ 2-3%, see Thum et al. 2003, comparable to our sensitivity as stated elsewhere). If some detections from sources with weak p_L are

Table 1. Stars observed in this work. The stellar type is derived from the literature as are the mass loss rates (e.g. Loup et al. 1993) and the period (e.g. AAVSO data).

Stars	RA (J2000)	DEC (J2000)	Type	V_{LSR} [km s^{-1}]	dM/dt [$M_\odot$/yr]	Period [days]	Optical phase
IRAS 18055-1433	18:08:23.20	-14:32:43.0	IR late-type	180	unknown	unknown	
IRAS 18158-1527	18:18:41.50	-15:26:25.0	IR late-type	20	unknown	unknown	
IRAS 18204-1344	18:23:17.90	-13:42:46.0	IR Supergiant (M8)	45	$4.2\ 10^{-6}$	unknown	
W And	02:17:32.96	44:18:17.8	Mira (S6,1E-S9,2E/M4-M1)	-35	$8.0\ 10^{-7}$	395.9	0.62
AU Aur	04:54:15.00	49:54:00.3	Mira (C6-7,3E(N0E))	8	$1.1\ 10^{-7}$	400	0.17
NV Aur	05:11:19.43	52:52:33.6	Mira (M10)	2	$7.6\ 10^{-6}$	635	
R Aur	05:17:17.69	53:35:10.0	Mira (M6.5E-M9.5E)	-3	$9.8\ 10^{-7}$	457.5	0.83
RU Aur	05:40:07.89	37:38:10.7	SRb (M7E-M9E)	-35	unknown	466.4	0.25
TX Cam	05:00:51.15	56:10:54.0	Mira (M8-M10)	10	$2.5\ 10^{-6}$	557.4	0.70
V Cam	06:02:32.30	74:30:27.1	Mira (M7E)	8	$1.6\ 10^{-6}$	522.4	0.91
R Cnc	08:16:33.83	11:43:34.6	Mira (M6E-M9E)	14	$6\ 10^{-7}$	361.6	0.33
W Cnc	09:09:52.63	25:14:53.8	Mira (M6.5E-M9E)	38	$3.1\ 10^{-8}$	393.2	0.76
VY CMa	07:22:58.33	-25:46:03.2	Red Supergiant (M3-M4II)	15	10^{-5}	400	0.37
S CMi	07:32:43.08	08:19:05.3	Mira (M6E-M8E)	52	$4.1\ 10^{-8}$	332.9	0.35
R Cas	23:58:24.79	51:23:19.5	Mira (M6E-M10E)	27	$1.1\ 10^{-6}$	430.4	0.66
S Cas	01:19:41.97	72:36:39.3	Mira (S3,4E-S5,8E)	-28	$3.1\ 10^{-6}$	612.4	0.98
T Cas	00:23:14.25	55:47:33.3	Mira (M6E-M9.0E)	-7	$5.1\ 10^{-7}$	444.8	0.22
T Cep	21:09:31.85	68:29:27.6	Mira (M5.5E-M8.8E)	-1	$1.4\ 10^{-7}$	388.1	0.94
R Com	12:04:15.20	18:46:56.7	Mira (M5E-M8EP)	-3	10^{-7}	362.8	0.43
S CrB	15:21:23.96	31:22:02.7	Mira (M6E-M8E)	3	$5.8\ 10^{-7}$	360.2	0.44
R Crt	11:00:33.87	-18:19:29.6	SRb (M7III)	10	$7.5\ 10^{-7}$	160	
χ Cyg	19:50:33.94	32:54:50.6	Mira (S6,2E-S10,4E)	10	$5.6\ 10^{-7}$	408	0.37
UX Cyg	20:55:05.40	30:24:53	irregular variable (M4E-M6.5E)	1	$3.2\ 10^{-6}$	565	0.77
R Hya	13:29:42.82	-23:16:52.9	Mira (M6E-M9E(TC))	-8	$1.4\ 10^{-7}$	388.8	0.95
W Hya	13:49:02.03	-28:22:03.0	SRa (M7.5E-M9EP)	42	$8.1\ 10^{-8}$	361	0.83
X Hya	09:35:30.26	-14:41:28.5	Mira (M7E-M8.5E)	26	$4.8\ 10^{-8}$	301.1	0.0
R Leo	09:47:33.49	11:25:44.0	Mira (M6E-M8IIIE-M9.5E)	0	10^{-7}	309.9	0.84
W Leo	10:53:34.44	13:42:54.4	Mira (M5.5E-M7E)	49	unknown	391.7	0.45
R LMi	09:45:34.28	34:30:42.8	Mira (M6.5E-M9.0E)	2	$2.8\ 10^{-7}$	372.2	0.56
T Lep	05:04:50.84	-21:54:16.2	Mira (M6E-M9E)	-29	$7.3\ 10^{-9}$	368.1	0.59
RS Lib	15:24:19.78	-22:54:39.7	Mira (M7E-M8.5E)	7	$1.8\ 10^{-8}$	217.6	0.28
Ap Lyn	06:34:34.90	60:56:33.0	Mira (M9)	-23	$4.9\ 10^{-6}$	unknown	
U Lyn	06:40:46.49	59:52:01.6	Mira (M7E-M9.5E)	-10	unknown	433.6	0.13
GX Mon	06:52:46.90	08:25:20.0	Mira (M9)	-9	$5.4\ 10^{-6}$	527	
SY Mon	06:37:31.28	-01:23:43.6	Mira (M6E-M9)	-57	unknown	422.2	0.18
V Mon	06:22:43.58	-02:11:43.2	Mira (M5E-M8E)	5	unknown	341	0.0
U Ori	05:55:49.18	20:10:30.7	Mira (M6E-M9.5E)	-38	$2.8\ 10^{-7}$	368.3	0.24
RR Per	02:28:28.73	51:16:21.1	Mira (M6E-M7E)	7	unknown	389.6	0.17
S Per	02:22.51.76	58:35:11.4	SRc (M3IAE-M7)	-40	$1.4\ 10^{-6}$	822	0.58
QX Pup	07:42:16.83	-14:42:52.1	PN (M6)	34	$1.1\ 10^{-4}$	unknown	
Z Pup	07:32:38.06	-20:39:29.2	Mira (M4E-M9E)	4	unknown	508.6	0.74
VX Sgr	18:08:04.05	-22:13:26.6	Red Supergiant (M4EIA-M10EIA)	6	$5.5\ 10^{-6}$	732	0.38
AH Sco	17:11:17.02	-32:19:30.7	SRc (M4E-M5IA-IAB)	-7	10^{-6}	713.6	0.98
RR Sco	16:56:37.85	-30:34:48.1	Mira (M6II-IIIE-M9)	-28	$1.1\ 10^{-8}$	281.4	0.35
R Ser	15:50:41.74	15:08:01.4	Mira (M5IIIE-M9E)	28	$2.6\ 10^{-7}$	356.4	0.20
S Ser	15:21:39.53	14:18:53.1	Mira (M5E-M6E)	20	$< 2.2\ 10^{-7}$	371.8	0.76
WX Ser	15:27:47.30	19:33:48.0	Mira (M8E)	7	$2.6\ 10^{-6}$	425.1	0.30

from a bad or uncertain pointing, they naturally induce a value of p_C which is weaker than p_L.

A strong instrumental polarization in Stokes V would be rather due to a bad phase tracking (the IF polarimeter works in a manner quite similar to that of an adding interferometer, and good phase tracking is essential). From several tests (Thum et al. 2003, Wiesemeyer, Thum & Walmsley 2004), we know that polarization seen for weak SiO components with (Q,U,V)= (+ - -), (- - +) or (- + -) is instrumental polarization. We see that signature for only 3 objects (R Crt, R UMi and RT Vir). Some instrumental polarization may thus contaminate the observations of these objects.

All instrumental parameters were carefully calibrated through specific procedures described in Thum et al. (2003). The error on $p_{L,C}$ is $\leq 2-3$ %.

Table 1. (-continued). Stars observed in this work. The stellar type is derived from the literature as are the mass loss rates (e.g. Loup et al. 1993) and the period (e.g. AAVSO data).

Stars	RA (J2000)	DEC (J2000)	Type	V_{LSR} [km s^{-1}]	dM/dt [$M_\odot$/yr]	Period [days]	Optical phase
IK Tau	03:53:28.80	11:24:22.7	Mira (M6E-M10E)	35	4.4 10^{-6}	470	0.80
R Tau	04:28:18.00	10:09:44.8	Mira (M5E-M9E)	14	6.5 10^{-8}	320.9	0.68
RX Tau	04:38:14.57	08:20:09.4	Mira (M6E-M7E)	-41	$< 5.810^{-8}$	331.8	0.13
R Tri	02:37:02.32	34:15:51.4	Mira (M4IIIE-M8E)	57	1.1 10^{-7}	266.9	0.0
R UMi	16:29:57.87	72:16:49.0	SRb (M7IIIE)	-6	unknown	325.7	0.35
S UMi	15:29:34.66	78:38:00.2	Mira (M6E-M9E)	-42	unknown	331	0.68
R Vir	12:38:29.95	06:59:19.0	Mira (M3.5IIIE-M8.5E)	-26	unknown	145.6	0.12
RS Vir	14:27:16.39	04:40:41.1	Mira (M6IIIE-M8E)	-12	3.8 10^{-7}	353.9	0.61
RT Vir	13:02:37.96	05:11:08.5	SRb (M8III)	18	7.4 10^{-7}	155	0.60
S Vir	13:33:00.11	-07:11:41.0	Mira (M6IIIE-M9.5E)	12	4.1 10^{-7}	375.1	0.27

SiO (v=1, J=2-1) line observations at 86.243442 GHz were carried out towards 57 stars in August and November 1999 with the IRAM 30m radiotelescope. The pointing was regularly checked directly on the star itself (for the vast majority of objects). In order to obtain flat baselines, we used the wobbler switching mode. The system temperature of the SIS receiver ranged from 110 to 170 K. The front-ends were the facility receivers A100 and B100, and the back-end was the autocorrelator. The lines were observed with a spectral resolution of 0.3 km s^{-1} . The integration times were 4-10 minutes using the wobbler switching. The forward and main beam efficiencies were respectively 0.92 and 0.77 at 3 mm. (Additional SiO (v=1, J=5-4) line observations at 215.596 GHz were also performed in most stars studied here; results will be reported elsewhere.)

Our source sample (see Table 1) consists of 43 Miras, 7 Semi-Regular stars (hereafter *SR*), 2 IR late-type stars, 1 irregular variable, 3 supergiants and 1 Planetary Nebula (QX Pup) selected from our SiO maser master catalogue (Herpin & Baudry, private communication). Coordinates and the main characteristics of the objects are given in Table 1. Nearly 60 % of stars in this table have been observed with the HIPPARCOS satellite and have thus excellent optical positions; such positions have been adopted in our work.

3. Results: Polarization Study

3.1. Individual results

Values of the polarization level presented here (see Table 2) are those measured for the different components within the SiO maser emission profile for each star. Examples are given in Fig.2 for a few stars. The complete Figure 2 with all the observations is available in electronic form at http://www.edpscience.org. Only the well identified components are considered (distinct peaks or strong wing emission well separated from the bulk emission, according to the noise). Some interesting cases are briefly presented below.

Some profiles show isolated emission red/blue-shifted from the main emission which are more strongly circularly polarized (e.g. IRAS 18204-1344). These peculiar characteristics imply a different spatial origin for the main and higher/lower velocity components. Sometimes the circular polarization is regularly varying across the profile (e.g. R Leo), but sometimes not.

In T Lep, the SiO emission shows two peaks linked by a plateau; the circular polarization is linearly varying across the profile from -11 to 10 % (see Fig. 2). Several objects (e.g. S UMi, IK Tau) show the same p_C pattern.

The IR late-type source IRAS18158-1527 exhibits a complex profile with several well defined components, each of them differently polarized indicating a complex maser structure with probably different maser spots contributing to the whole emission. The red wing emission is highly polarized (43 %). Such a complex multi-component maser line profile and "semi-circle", convex, p_C pattern appear to be characteristic of SR objects (see other similar objects in our sample and R Crt in Fig. 2). Nevertheless, the circular polarization pattern observed in the Mira star U Lyn is a convex profile as encountered in SR objects.

One of the most studied Mira star is R Leo. The profile is made of a strong emission with a blue broad line wing. Main and linewing emissions are strongly polarized (respectively negative and positive $p_C \sim 9 - 10$ %). R Leo is a very well studied object exhibiting a bipolar jet throughout its envelope. The clear symmetry observed between the positive and negative circular polarization patterns in the main and wing line emissions suggests that the maser emission comes from the jet lobes. We note that the Mira star RS Lib exhibits an emission and polarization pattern similar to that observed in R Leo. R Leo and RS Lib may have the same spatial structure.

3.2. Analysis

The circular polarization level in several of our objects has already been measured by Kemball & Diamond (1997) or Barvainis, McIntosh & Predmore (1987). For TX Cam and W Hya, our results are consistent with previous observations:

- in TX Cam, the bulk of the emission is weakly circularly polarized while its wings show $p_C \sim 3 - 6$% in good agreement with the VLBI observations of Kemball & Diamond in 1997 who derived an average value of $p_C \sim 3 - 5$%;
- in the Semi-Regular object W Hya, the central emission is weakly polarized (± 2 %), while the wings and secondary

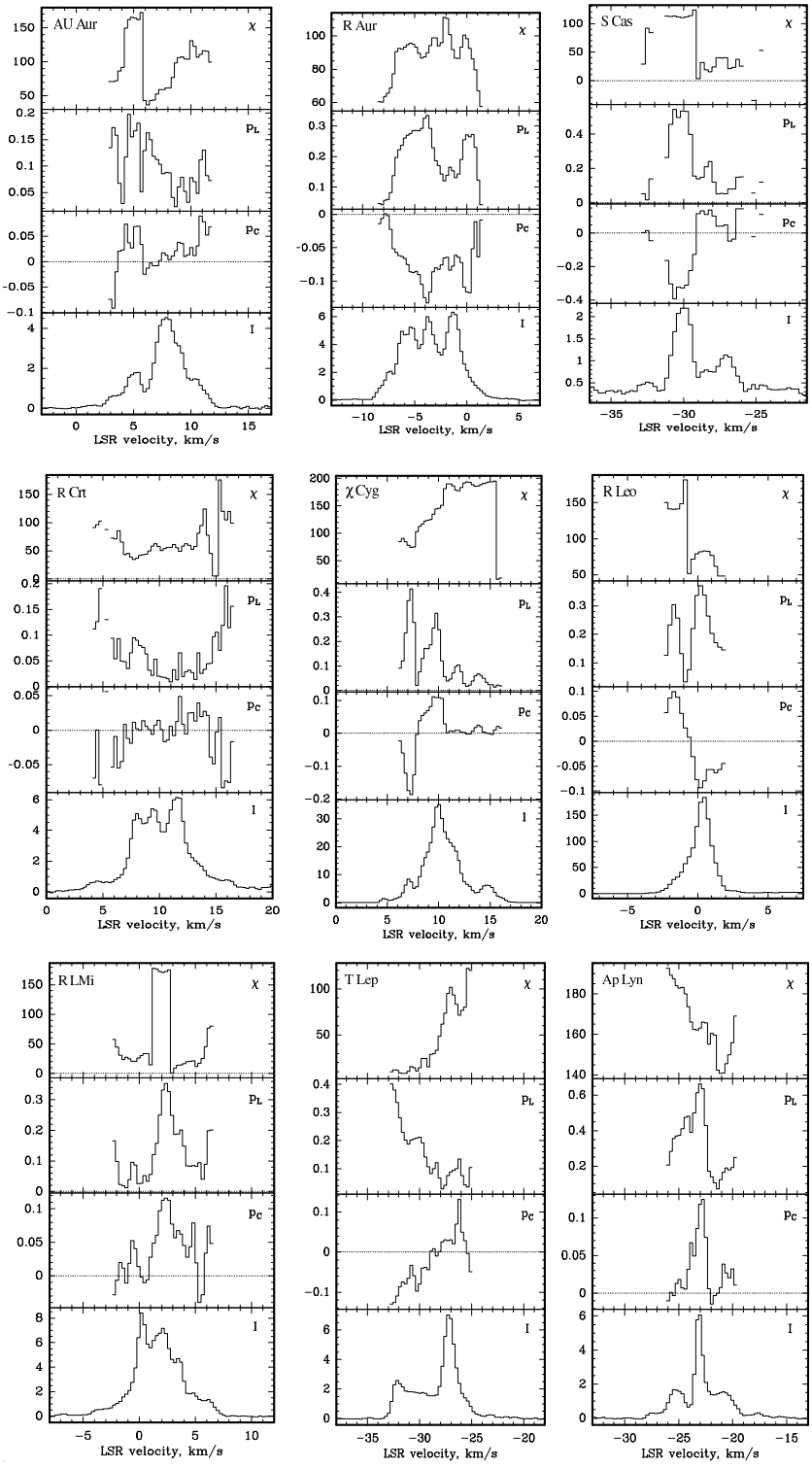


Fig. 2. Position angle of polarization (χ) in degrees, linear (p_L) and circular (p_C) polarization levels and intensity ($I = Ta^{\star}$ in Kelvin; the conversion factor is 6 Jy/K) for the SiO emission observed in several stars.

peaks show p_C= 2-6 %), which is consistent with the 5 % of Barvainis, McIntosh & Predmore (1987).

On the contrary, the circular polarization level we derive in VY CMa, R Cas, R Leo, and VX Sgr is different from levels measured by Barvainis, McIntosh & Predmore (1987), respectively 1-4, 2-6, 9-10 and less than 3 % while they found respectively 6.5, 1.5, 2.4 and 8.7 %. This difference is significant and may be due to variability over the fifteen intervening years. Indeed time variability of the polarization remains an open question in the field. Glenn et al. (2003) have shown that the individual maser feature lifetime ranges from a few months or less to

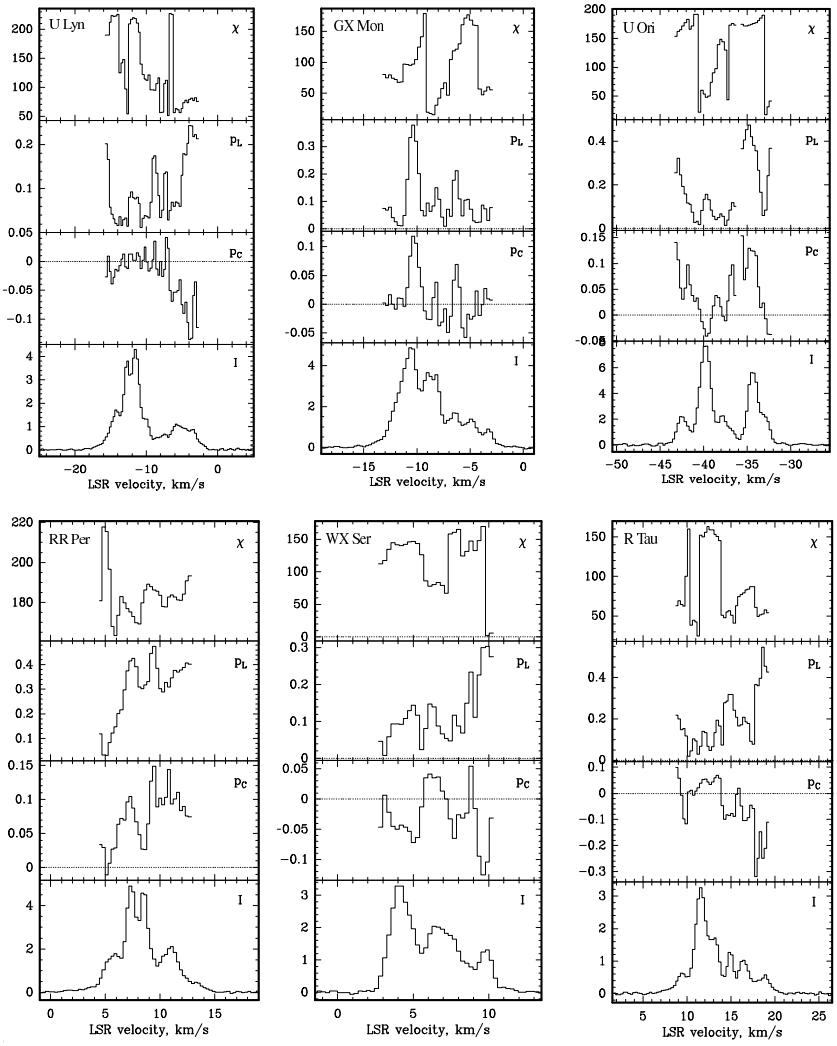


Fig. 2. (-continued). Position angle of polarization (χ) in degrees, linear (p_L) and circular (p_C) polarization levels and intensity ($I = Ta^{\star}$ in Kelvin) for the SiO emission observed in several stars.

more than 2 years, i.e. the characteristic time over which the *Q* and *U* spectral features persist. The average linear polarization is 23 % in Glenn et al. sample with a typical dispersion of 7%. Cotton et al. (2004) have comparable epoch spacing and do not conclude on the variability. Our observations were repeated at intervals of a few months (August and November 1999) and the polarization tends to remain stable between the two epochs.

We emphasize that we cannot spatially distinguish with a single dish radiotelescope between the different maser spots producing the SiO profile (various masers spots contribute in the various features observed at a given velocity). The whole SiO maser emission region, hence all the maser cells, lie within the 29 arcseconds of the 30m (but not necessarily with a uniform distribution) while the SiO emission covers less than 40 milliarseconds in TX Cam (Kemball & Diamond 1997) and thus everything is beam averaged. This means that any conclusion on the geometry of the objects observed here would be much uncertain. Only global trends or global geometry can be discussed. One of the consequences of this spatial resolution problem is that if the polarization vectors are distributed isotropically around the object, the average polarization level that we measure is zero, even if the maser emission produced in each SiO cell is well polarized.

A global analysis of our data in Table 2 shows the following. We find that p_L varies between 0 and 70 %, and p_C between 0 and ±43 %. Hence, polarization vectors are not distributed isotropically. Emission from Mira-type objects clearly tends to have a relatively high linear ($< p_L >_{Mira} \simeq 30\%$, $< p_L >_{SR} \simeq 11\%$) and circular polarization ($< p_C >_{Mira} \simeq 9\%$, $< p_C >_{SR} \simeq 5\%$). Note that the emission from the PN QX Pup is highly polarized, and, on the contrary, maser emission from supergiants shows very weak polarization ($< p_L >= 5\%$, $< p_C >= 2\%$), with the exception of one maser component in S Per. Moreover, all observations show that the polarization level varies across the maser line profile (see Fig. 2), i.e. the different spectral components of the maser emission producing the profile are coming from different localizations in the SiO shell and have different polarization levels. The highest polarization level for one object can be encountered either in the main peak, or in the other components.

Semi-Regular objects (RU Aur, R Crt, W Hya, S Per, AH Sco, R UMi, RT Vir) have a common circular polarization pattern with the central main emission unpolarized and other peak emission or wings being strongly polarized: a characteristic "semi-circle" (i.e. convex shape) pattern for p_C is observed (see R Crt in Fig. 2). The infrared late-type star IRAS18158-1527 exhibits a similar pattern, thus suggesting that this star is a semi-regular.

A group of objects (W And, NV Aur, T Cas, R Com, T Lep, IK Tau, S Ser, S UMi) shows approximately the same p_C pattern (see T Lep in Fig. 2); the circular polarization varies linearly across the line profile from a positive value to a negative one (or the contrary). The only common spectral characteristic of the SiO emission from these stars is the presence of an plateau-like emission on top of which the narrow emission peaks are located.

4. Discussion

In this section, we first discuss our source sample in the frame of the 2-color diagram. Then, we briefly summarize the existing SiO maser polarization theories. Finally, we discuss our data set in this context and estimate the stellar magnetic field strength.

4.1. 2-color diagram

Stars of our sample can be plotted in a [12]-[25], [25]-[60] color-color diagram (van der Veen & Habing 1988; [12], [25] and [60] stand respectively for 12, 25 and 60 microns IRAS-fluxes). This diagram is partitioned into several regions (see Fig. 3) defined by van der Veen & Habing as follows: Region I, oxygen-rich non variable stars without circumstellar shells; Region II, variable stars with young O-rich circumstellar shells; Region IIIa, variable stars with more evolved O-rich circumstellar shells; Region IIIb, variable stars with thick O-rich circumstellar shells; Region IV, variable stars with very thick O-rich circumstellar shells; Region V, Planetary Nebulae and non-variable stars with very cool envelopes; Region VIa, non variable stars with relatively cold dust at large distance; Region VIb, variable stars with relatively hot dust close to the star and relatively cold dust at large distance; Region VII, variable stars with more evolved C-rich circumstellar shells.

On Fig. 3 are represented the linear and circular polarization level for the main SiO emission component from each star. Most of the objects in our sample fall in regions II and IIIa and do not show particular characteristics, except for S Cas (an S-type star) where the circular polarization is high. Mira-type stars are in regions I, II, IIIa and VII. IR late-type objects are in VIb and VII. The SRa semi-regular variable W Hya is in I, while the SRb stars lie in IIIa (RU Aur, RT Vir, R Crt), II (R UMi), and Src in IIIa (S Per) and VII (AH Sco). The Red Supergiants, VY CMa and VX Sgr, and the IR supergiant IRAS 18204-1344 lie in VII. Objects in Region VII do not exhibit strong polarization compared to other objects, perhaps because of their more C-rich circumstellar shells (e.g. AU Aur) or because of the presence of hot dust close to the star implying less SiO abundance and thus weaker emission, making the polarization measurement less significant. The presence of hot dust may also influence the pumping of the SiO molecules and thus the polarization level; the optically thick, hence isotropic, radiation field of hot dust can assist the collisional pumping. This could apply to UX Cyg (an irregular variable), IRAS 18055-1433 and IRAS 18158-1527 in region VIb. QX Pup in region V is a PN and exhibits strong polarized emission. Note that IRAS 18055-1433 and IRAS 18158-1527 show very strong circular polarization in their line wings. We may conjecture here that wing emission comes from more outer layers than those where the main line is excited (Herpin et al. 1998); as a consequence, the SiO cells giving rise to wing emission are less influenced by the presence of hot dust (hot dust preferably lies in the inner layers).

4.2. The SiO maser polarization theory

Since SiO is non-paramagnetic, the Zeeman splitting $g\nu_B$ (g is the Land factor) is much less than the Doppler width. Moreover, the degree of saturation is the ratio of the rate R for stimulated emission to the loss rate Γ (usually Γ is approximated by the inverse radiation lifetime for a vibrational transition, $\Gamma \simeq 5$ s^{-1} for SiO masers, Wiebe & Watson 1998). Hence, if $R \geq \Gamma$, the maser is saturated. In fact, in the Orion case Plambeck et al. (2003) show that, despite the radiation beam angle is unknown, the 86 GHz SiO maser is saturated. The maser is saturated if the angle averaged intensity $J = \frac{I\Omega_b}{4\pi}$ (Ω_b is the beaming solid angle) is larger than the saturation intensity J_S; J_S is a theoretical quantity. The saturation depends on the angle into which the radiation is beamed, but this angle is unknown (Watson & Wyld 2001), thus J cannot be directly measured (even if I is measurable when the maser is resolved, the beaming angle Ω is not an observable).

For more than one decade, two schools have come up against each other to explain SiO maser emission. SiO polarization theory is described in: (i) Watson (e.g. Watson & Wyld 2001, Wiebe & Watson 1998, Nedoluha & Watson 1994); (ii) Elitzur (2002, 1998, 1996, 1994).

The main difference between the two approaches rests in the pumping mechanisms. While anisotropic pumping associated with a weak field produces high p_L and quite significant p_C in Watson's model, a strong magnetic field is necessary with the more classical pumping mechanisms used in Elitzur's model. Details about both models can be found in the Elitzur's review (2002).

We may summarize the main characteristics of Watson's model as follows:

- non-Zeeman effect;
- anisotropic pumping;
- no direct relation between p_C and B. An estimation of B can only be derived through complete calculation of the radiative transfer. Nevertheless, when maser saturation is not important, the "thermal" spectral line equation $\frac{V}{\delta I/\delta v} = \alpha B \cos\theta$ is applicable (Fiebig & Güsten 1989); I is the intensity with respect to Doppler velocity v, θ is the angle between B and the line of sight, α is a constant;
- the Zeeman splitting parameter $g\Omega$ (in frequency units $g\Omega = 1.5B[mG]s^{-1}$ for SiO masers) is $\simeq R$;

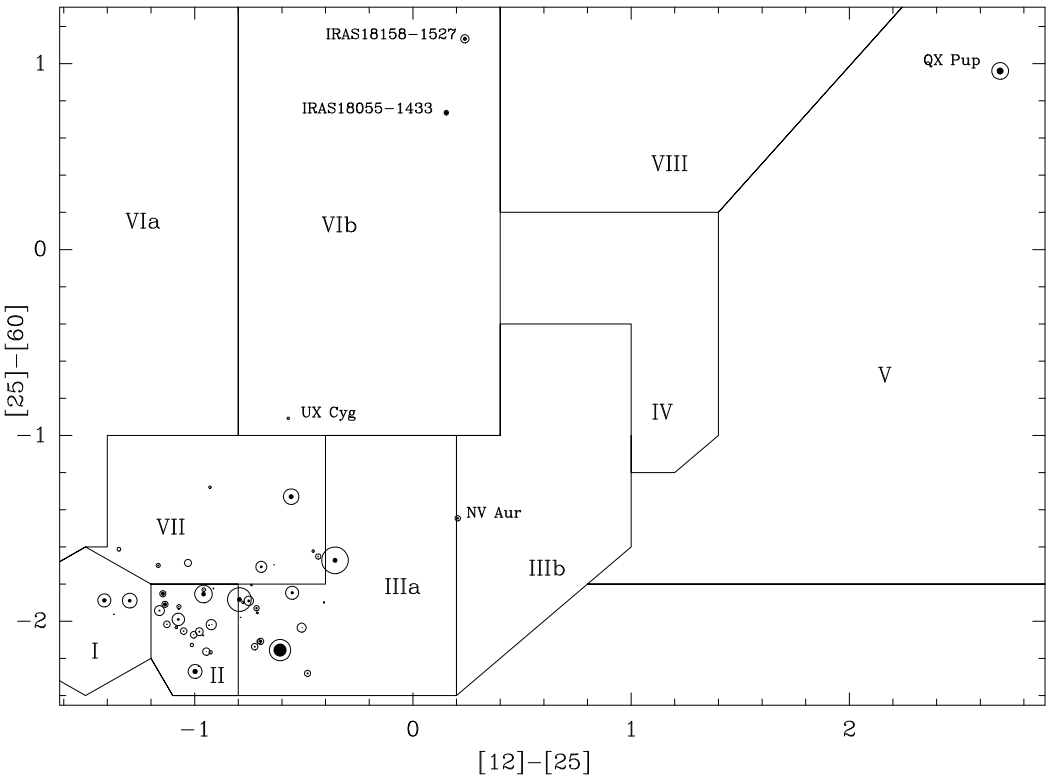


Fig. 3. Two-color diagram for our sample. The size of the empty and filled circles for each star are proportional to respectively the linear and absolute circular polarization level measured for the main peak of SiO emission.

– saturated or unsaturated maser (saturated maser increases p_C);
– linear correlation between p_L and p_C, and high p_L is needed;
– intensity dependent circular polarization;
– B of a few 10 mG varying as $r^{-2,3}$ throughout the envelope.

In contrast with Watson's work, Elitzur's model is based on the Zeeman effect and the exponential maser growth in the unsaturated phase; the polarization characteristics are preserved as the radiation is amplified into the saturated regime. This model was improved several times (Elitzur 1994, 1996, 1998) and takes into account the anisotropic pumping. The magnetic field generates circular polarization and the main pumping mechanism for the SiO maser is a "classical" radiative-collisional process. For saturated masers, a direct relation between p_C and B is obtained from simple calculations. The ratio x_B of the Zeeman splitting $\Delta\nu_B$ to the Doppler linewidth $\Delta\nu_D$, can be determined (Elitzur 1996) from v_{peak}, the ratio of the Stokes parameter V/I at a given peak feature:

$$x_B = \frac{3\sqrt{2}}{16}\, v_{peak} \cos\theta \tag{7}$$

Following Barvainis, Mc Intosh & Predmore (1987) and Elitzur (1996) we arbitrarily take $\theta \simeq 45°$

$$\Rightarrow x_B = \frac{3}{16}\, v_{peak} \tag{8}$$

$$\Rightarrow x_B = 0.1875\ 10^{-2}\, m_C \tag{9}$$

where m_C is the polarization fraction in percentage (i.e. 100 p_C). Moreover:

$$x_B = 14 g \lambda \frac{B}{\Delta v_D} \tag{10}$$

where g is the Landé factor with respect to the Bohr magneton, λ the transition wavelength in cm, B the field in Gauss and Δv_D the Doppler width in kms^{-1}. Thus,

$$B = 0.1875\ 10^{-2}\ \frac{\Delta v_D}{14 g \lambda}\ m_C \tag{11}$$

With $g \simeq 10^{-3}$, $\Delta v_D = 1$ km s^{-1} and $\lambda = 0.2877$ cm, we derive:

$$B \simeq 0.46\, m_C \tag{12}$$

This model predicts that there is no correlation between p_C and p_L (see also Watson & Wyld 2001); such a mechanism leads to an inferred magnetic field of a few Gauss to 10 Gauss for the SiO maser zone, the field hence varying as $r^{-1,2}$ across the envelope.

4.3. Theory against present observations

The relevance of the two different polarization theories can be assessed via a few observational checks:

– dependence of circular polarization on intensity;
– linear correlation between p_C and p_L;
– Zeeman effect, i.e. spectral shape of the Stokes parameter V;

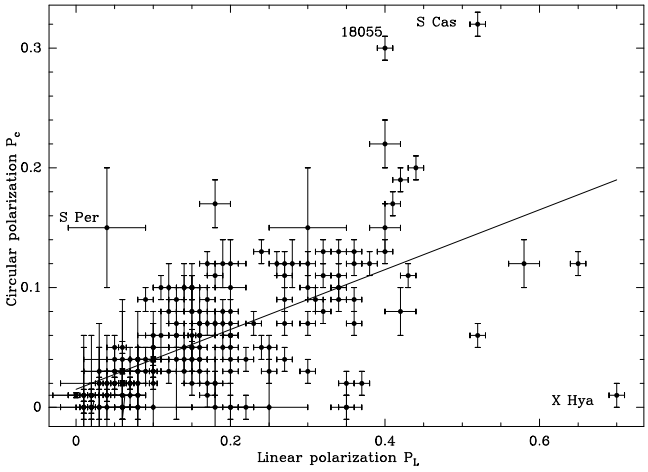


Fig. 4. Absolute fractional polarization p_c versus p_L for the whole sample and all maser components (wings + center). A regression fit is shown: $p_C \simeq 0.015 + 0.25 p_L$

– coherence of B strength values inferred from OH and H_2O observations.

As we do not resolve the maser emission into individual spatial components, our current data set is biased by the beam averaging. Therefore, some effects cannot be tested with our data. In the Zeeman effect case, the spectral shape of the Stokes parameter *V* must follow an antisymmetric *S* curve with sharp reversal at line center (Elitzur 1996). Unfortunately the doppler width is less than the resolution of the observations and we cannot conclude.

We may look for any correlation between p_C and p_L. As shown in Figs. 2 and 3, it first appears that in all cases p_L is larger than p_C as is predicted by all models. More precisely, p_C is noticeable if and only if p_L is high. If we plot the values of p_C and p_L derived for all maser components in this work (Fig. 4) and make a regression fit to our data we obtain $p_C \simeq 0.015 + 0.25\ p_L$. The circular polarization level tends to vary approximately linearly with p_L in agreement with the fact that no p_C is detected towards sources with a marginal p_L detection. Note that in Fig. 4, four objects, S Per, IRAS18055-1433, S Cas and χ Hya, do not follow the same general trend observed for the rest of the sample. (The case of the Supergiant S Per, however, is an exception as it exhibits substantial p_C while $p_L < p_C$.) This observation may in fact favour Watson's model. It must be stressed again that the beam-averaged polarization that we measure makes any conclusion uncertain. In fact, due to this averaging, we should observe no correlation at all, even if such one would exist !

As mentioned earlier (see Section 3.2) we observe relatively high circular polarization rates in several stars ($< p_C >_{Mira} \simeq 9\%$, $< p_C >_{SR} \simeq 5\%$). These values are larger than those predicted from Watson's model (e.g. Nedoluha & Watson 1994). We also have not been able to find any correlation of p_C with total intensity. Finally, although we adopt the Zeeman case to derive the magnetic field strength (see Section 4.5), we cannot conclude firmly from present observations which maser theory prevails for SiO emission.

4.4. Magnetic field in AGB stars

A better knowledge of the stellar magnetic field strength is crucial to understand the last stages in the life of an Asymptotic Giant Branch (hereafter AGB) star. These stages are characterized by a high mass loss process driven by the radiation pressure; they are also influenced by the magnetic field (Palen & Fix 2000, Blackman, Frank & Welch 2001, and references therein). A strong magnetic field may rule the mass loss geometry; in particular, it could be the cause of a higher or lower mass-loss rate in the equatorial plane (Soker 2002), and thus determine the global shaping of these objects. But, as the direct dynamical effect of the magnetic activity is much lower than that of the wind (although in local spots the magnetic field can be dominant), the role of the magnetic field might be indirect. Moreover, the observed high mass loss rates are hardly explained by a single process and need a combination of several factors such as rotation, the presence of a companion (binary stars, with our without common envelope, exhibiting mass transfer or tidal effects are common; Soker 1997) and a magnetic field. During its quick transition to the PN stage, the AGB star will completely change its geometry: the quasi-spherical object becomes axisymmetrical, point-like symmetrical or even shows higher order symmetries (Johnson & Jones 1991, Sahai & Trauger 1998, Balick & Frank 2002). The classical or generalized *Interacting Stellar Winds* (hereafter ISW or GISW) models (Kwok 2000, Soker & Livio 1989, Morris 1987) try to explain this shaping, but have serious difficulties in producing complicated structures with peculiar jets or ansae (e.g., CRL 2688, Delamarter 2000) and do not fully address the origin of the wind. Furthermore, recent X-ray studies with the Chandra satellite do not completely agree with GISW predictions for temperatures (Guerrero et al. 2001).

Some recent studies tend to demonstrate the importance of the magnetic field in evolved objects. Bujarrabal et al. (2001) show that for 80% of the PPNe in their sample the fast molecular flows have too high momenta to be powered by radiation pressure only (1000 times larger in some cases) what may be explained by magnetic field. Moreover, X-ray emission found in evolved stars (e.g. Hünch, Schmitt & Schröder 1998) may indicate the presence of a hot corona that possibly results from magnetic activity. Very recently, magnetic field was discovered for the first time in central stars of PN (Jordan et al. 2005) and estimated to kiloGauss, much stronger than what we find here from our SiO data in QX Pup.

New models involving the magnetic field have been developed trying to explain the morphology changes of an object during its transition from the AGB stage to the PN stage; B plays the role of a catalyst and of a collimating agent. The most simple models are based on a moderately weak magnetic field alone ($B \simeq 1$ Gauss at the stellar surface, a few 10^{13} cm, i.e. at a radiis of a few AU, Soker 1998). The influence of B is stressed by the work of Smith et al. (2001) and Greaves (2002) in VY CMa. But the role of B can only be decisive when its energy density is greater than the radiative pressure, i.e. when B is greater than around 10 G close to the stellar surface in the SiO region (see Soker & Zaobi, 2002). Arguing that such a strong field may be very unusual, Balick & Frank (2002) explain that

B alone cannot produce the observed structures, and a combination of several factors has thus to be considered (rotation, magnetic field and presence of a companion).

Soker & Harpaz (1992) first proposed a model with a weak magnetic field ($\leq$ 1 G) and included a slow rotation together with the presence of a companion to transform the envelope (and lead for example to the peculiar geometry observed in NGC 6826 or NGC 6543). Even if the star were not binary, the influence of B is probably important locally (Palen & Fix 2000). A significant magnetic field can form cold spots on the star's surface and a slow rotation of the star can then increase the field strength to build up a dipolar magnetic field varying as $1/r^3$ (Matt et al. 2000); such a field is stronger at the equator and may thus lead to an axisymmetrical mass loss.

The main argument against the dominant influence of the magnetic field on the shaping of the circumstellar envelope is that a strong field seems to be necessary to dominate the dynamics of the gas. However, several authors (Pascoli 1985, 1992, 1997, Chevalier & Luo 1994, García-Segura 1997, Gurzadyan 1997, Delamarter 2000) have demonstrated the strong influence of a reasonable toroïdal magnetic field embedded in the normal radiation-driven stellar wind (*Magnetic Wind Bubble* theory, hereafter *MWB*). This field has a strength between a few Gauss and a few 10 Gauss at a few stellar radii (the SiO region is believed to be at $\sim 10^{14}$ cm or $\sim 7-10$ AU), varies as $1/r^2$, then as $1/r$ at larger radii; therefore $B \sim 1$ mG at $10^{16,17}$ cm or 700-7000 AU. These results are confirmed by the simulations of García-Segura, Lopez & Franco (2001) for the PN He 2-90. Even if the origin of the wind is not explained by these models, it seems clear that a magnetic field is essential to generate fast collimated outflows (Kastner et al. 2003).

There are many models of magnetic jet production and collimation and some, or all of them, are applicable to various star geometries. One most interesting study was performed by Blackman, Frank & Welch (2001) in which the magnetic field emerges from the AGB stellar core and the resulting 1G field helps to collimate the radiation-driven wind or a stronger, more anisotropic, magnetically driven wind.

4.5. Magnetic field in our sample

The exact interpretation, in terms of magnetic field, of our observations depends on the adopted specific SiO maser model (see Sections 4.2 and 4.3). From the current knowledge of the strength of the magnetic field in the OH and H_2O layers we expect $B_{//}$ of a few Gauss at least in the SiO maser region (see also Kemball & Diamond 1997), i.e. at 5-10 AU from the central object. This tends to invalidate Watson's model, and furthermore tends to agree with a field varying in $r^{-1,2}$ as predicted by Elitzur's model. However, Vlemmings et al. (2005) measured the circular polarization of the H_2O maser emission in a few evolved stars with the VLBA observations and showed that the magnetic field is either a solar-type field (with a r^{-2} field strength dependence) or a dipole magnetic field (with a r^{-3} dependence) in their sample.

In the following, we decide to use Elitzur's theory (Zeeman case) to infer magnetic field strength from the circular polarization levels. From equation (12), we thus calculate the mean value of the magnetic field $B_{//}$ for each star and give results in Table 3.

For our sample $B_{//}$ is between 0 and 20 Gauss, with a mean value of 3.5 G. This value combined with the strength of the field in more outer layers of the envelope (OH and H_2O masers) agrees with a B field variation law in $1/r$, closer to Elitzur's model. As explained in the Introduction and in Section 4.4, B alone can be the main agent to shape the circumstellar envelope if its value is larger than around 10 Gauss. This means that only S Cas, RU Aur, IRAS 18055-1433 and IRAS 18158-1527 may have a *magnetic field ruled geometry* ($B > 10$ G in these objects). The rest of our sample shows that B is sufficiently strong to be dominant at this stage of the AGB star evolution, but it should be associated with rotation and the presence of a companion as suggested in models mentioned in Section 4.4. Despite our B measurements are beam averaged, they suggest in many cases that they are not too much (not orders of magnitude) below the critical value; local B values may exceed in many cases the critical value, and therefore participate in the shaping of the AGB envelopes. Our estimated values of B are consistent with the *MWB* theory (toroïdal magnetic field) or the model of Blackman, Frank & Welch (2001).

From Elitzur (1996) and our measurements $< p_C >_{Mira} \simeq 9\%$, $< p_C >_{SR} \simeq 5\%$, we can estimate (see Eq. (9) in Sect. 4.2) that $< x_B >$ is around 0.017 and 9.4 10^{-3} respectively for Mira-type objects and semi-regular variables. Moreover, according to Elitzur (1996, see Fig.2), there is no stationary physical solutions for propagation at $\sin^2\theta < \frac{1}{3}$ (i.e. at $\sin^2\theta < \frac{1}{3}$ the radiation is not polarized). As x_B is small (< 0.02), from Fig.2 of Elitzur (1996) we can estimate the volume of phase space in which propagation of linear polarization in a maser is possible or not ($\theta > 35.3°$ or $\theta < 35.3°$); we then calculate that the probability for a random magnetic axis to be aligned with a given direction (our line of sight) is better than 35.3°. Our present estimate is that around 18 %. Therefore, Elitzur's model predicts that 18.4 % of the SiO 86 GHz masers should not be linearly polarized, because such polarized masers cannot propagate if the magnetic field, although weak, is closer than 35.3° to the line of sight (propagation direction). Hence non polarized maser emissions do not imply no or weak magnetic field. In our sample, roughly 13 % of the SiO maser components have no detectable or very weak ($< 3\%$) polarization.

We looked without success for a possible correlation between the polarization rates and physical parameters such as the known envelope asymmetry, the presence of SiO maser high velocity linewings (see Herpin et al. 1998), or the mass loss rate. If the magnetic field plays an important role in the shaping of the object, one may expect to find a relationship between the strength of $B_{//}$ (thus p_C) and the geometry of the object. Unfortunately, no trend is clearly found in our data. Nevertheless it is known that radiative pressure is driving the wind in AGB objects and it is thus not surprising that we find no correlation between the B strength and a known asymmetry in our sample. Of course, our stellar sample would require new observations with sufficient spatial resolution (VLBI) to confirm the present results; the same type of study should also be conducted toward several Proto-PN and PN objects.

5. Conclusion

We have made a study of the SiO maser polarization in a representative sample of evolved stars, simultaneously measuring, for the first time, the 4 Stokes parameters. From our measurements we derive the circular and linear polarization levels and shows that, due to the beam averaging of our polarization measurements, we cannot firmly discriminate between the two dominant theories of SiO maser emission. In particular, VLBI observations of our source sample are absolutely necessary to distinguish between Zeeman or non-Zeeman theories. Nevertheless, the magnetic field strength was derived assuming Elitzur's model. B varies between 0 and 20 Gauss, with a mean value of 3.5 G. As a consequence, we suggest that the magnetic field plays a significant role in the evolution of these objects. Within the frame of the Zeeman theory the magnetic field could shape or even collimate the gas layers surrounding the AGB objects. Emission from Mira-type objects clearly tends to have a higher linear ($< p_L >_{Mira} \simeq 30\%$, $< p_L >_{SR} \simeq 11\%$) and circular polarization ($< p_C >_{Mira} \simeq 9\%$, $< p_C >_{SR} \simeq 5\%$). Basically, if there is a real correlation between p_C and the strength of the magnetic field, this trend may indicate that the magnetic field may be stronger in Mira objects than in Semi-Regular variables (at least in the inner layers of the circumstellar envelope).

To better understand the mechanisms at work with the magnetic field, complementary studies have to be conducted and in particular the presence of a companion has to be investigated in a large sample of objects. Of course VLBI maps of the magnetic field in these stars are essential. Another important objective is to investigate the evolution of the magnetic field and its influence during the transition from the AGB star phase to the PN stage.

Acknowledgements. The authors are grateful to M. Elitzur for reading and commenting on this paper. We also thank W.D. Watson for his useful comments and suggestions. The authors are indebted to the staff of the IRAM 30m telescope who most efficiently helped during the observations and to R. Mauersberger who closely followed part of these observations. Finally, we also thank the referee for several useful comments.

References

Balick B., Frank A. 2002, ARAA 40, 439
Barvainis R., McIntosh G., Read Predmore C. 1987, *Nature* 329, 613
Blackman E.G., Frank A., Welch C. 2001, ApJ 546, 288
Bujarrabal V., Castro-Carrizo A., Alcolea J., Sánchez Contreras C. 2001, A&A 377, 868
Bujarrabal V. 2003, Mass-losing pulsating stars and their circumstellar matter, edited by Y. Nakada, M. Honma and M. Seki. Astrophysics and Space Science Library, Vol. 283, Dordrecht: Kluwer Academic Publishers, p. 275 - 282
Chevalier R.A., Luo D. 1994, ApJ 435, 815
Cotton W.D., Mennesson B., Diamond P.J. et al. 2004, A&A 414, 275
Delamarter G.R. 2000, Ph-D thesis, University of Rochester
Elitzur M. 1994, ApJ 422, 751
Elitzur M. 1996, ApJ 457, 415
Elitzur M. 1998, ApJ 504, 390
Elitzur M. 2002, Astrophysical spectropolarimetry, Proceedings of the XII Canary Islands Winter School of Astrophysics, edited by J. Trujillo-Bueno, F. Moreno-Insertis, and F. Snchez. Cambridge, UK: Cambridge University Press, p. 225 - 264
Fiebig D., Güsten R. 1989, A&A 214, 333
García-Segura G. 1997, ApJ 489, L189
García-Segura G, Lopez J.A. & Franco J. 2001, ApJ 560, 928
Glenn J., Jewell P.R., Fourre R., Miaja L. 2003, ApJ 588, 478
Goldreich P., Keeley D.A., Kwan J.Y. 1973, ApJ 179, 111
Greaves J.S. 2002, A&A 392, L1
Guerrero M.A., Chu Y., Gruendl R.A. et al. 2001, ApJ 553, L55
Gurzadyan G.A. 1997, in *The Physics and Dynamics of Planetary Nebulae*, Berlin/Heidelberg/New York: Springe-Verlag
Herpin F., Baudry A., Alcolea J., Cernicharo J. 1998, A&A 334, 1037
Herwig F. 2003, Planetary Nebulae: Their Evolution and Role in the Universe, Proceedings of the 209th Symposium of the International Astronomical Union, edited by Sun Kwok, Michael Dopita, and Ralph Sutherland, p.61
Hünch M., Schmitt J.H.M.M., Scrhöder K.-P. 1998, A&A 330, 225
Jordan S., Werner K., O'Toole S.J. 2005, A&A 432, 273
Johnson D.R., Clark F.O. 1975, ApJ 197, L69
Johnson J.J., Jones T.J. 1991, AJ 101, 1735
Kastner J.H., Balick B., Blackman E.G. et al. 2003, ApJ 591, L37
Kemball A.J., Diamond P.J. 1997 ApJ 481, L111
Kwok S. 2000, in *The origin and Evolution of Planetary Nebulae*, Cambridge Astrophysics Series 31, Cambridge University Press edition
Loup C., Forveille T., Omont A., PAul J.-F. 1993, A&ASS 99, 291
McIntosh G.C., Predmore C.R., Moran J.M. et al. 1989, ApJ 337, 934
McIntosh G.C., Predmore C.R., Patel N.A. 1994, ApJ 428, L29
Matt S., Balick B., Winglee R., Goodson A. 2000, ApJ 545, 965
Monnier J.D., Millan-Gabet R., Tuthill P.G. et al. 2004, ApJ 605, 436
Morris M. 1987, PASP 99, 1115
Nedoluha G.E., Watson W.D. 1994, ApJ 423, 394
Palen S., Fix J.D. 2000, ApJ 531, 391
Pascoli G. 1985, A&A 147, 257
Pascoli G. 1992, PASP 104, 350
Pascoli G. 1997, ApJ 489, 946
Plambeck R.L., Wright M.C.H., Rao R. 2003, ApJ 594, 911
Rowan-Robinson M., Harris S. 1983, MNRAS 202, 767
Sahai R., Trauger J.T. 1998, AJ 116, 1357
Smith N., Humphreys R.M., Davidson K. et al. 2001, ApJ 121, 1111
Soker N., Livio M. 1989, ApJ 339, 268
Soker N., Harpaz A. 1992, PASP 104, 923
Soker N. 1997, ApJS 112, 487
Soker N. 1998, MNRAS 299, 1242
Soker N., Zoabi E. 2002, MNRAS 329, 204
Soker N. 2002, MNRAS 337, 1038
Szymczak M., Cohen R.J. 1997, MNRAS 288, 945
Thum C., Wiesemeyer H., Morris D., Navarro S., Torres M. 2003 *Proc. S.P.I.E.*, 4843, 272
Troland T.H., Heiles C., Johnson D.R., Clark F.O. 1979, ApJ 232, 143
van der Veen W.E.C.J., Habing H.J. 1988, A&A 194, 125
Vlemmings W., Diamond P.J., van Langevelde H.J. 2001, A&A 375, L1
Vlemmings W., van Langevelde H.J., Diamond P.J. 2005, A&A 434, 1029
Wallin B.K., Watson W.D. 1997, ApJ 481, 832
Watson W.D., Wyld H.W. 2001, ApJL 558, 55
Wiebe D.S., Watson W.D. 1998, ApJL 503, 71
Wiesemeyer H., Thum C., Walmsley C.M. 2004, A&A 428, 479

Table 2. Derived parameters of the different components of the SiO maser emission profile for each star. Only the well identified components are given (distinct peak or strong wing emission separated from the bulk emission). Note that the polarization is fractional. The δP is the rms derived from the p_C plot.

Source	v_{LSR} [km s^{-1}]	F_ν [Jy]	p_c	p_L	δp	χ [°]
18055-1433	180.6	1.02	-0.10	0.11	0.01	50
	182.7	1.7	-0.30	0.40	0.01	30
18158-1527	15.2	2.28	0.08	0.16	0.02	90
	17.5	1.86	-0.10	0.20	0.02	50
	21.7	1.74	0.11	0.15	0.02	170
	24.5	0.72	0.43	0.49	0.02	46
18204-1344	38.3	20.94	0.0	0.06	0.01	170
	41.5	33.18	0.03	0.06	0.01	150
	45.0	28.26	0.0	0.02	0.01	120
	49.0	3.90	0.04	0.08	0.01	110
	53.7	8.34	±0.07	0.06	0.01	120
W And	-38.0	4.98	0.08	0.20	0.01	70
	-35.9	16.32	-0.01	0.02	0.01	30
	-34.0	9.72	-0.07	0.16	0.01	175
	-32.3	2.52	0.12	0.28	0.02	140
AU Aur	3.4	3.72	-0.09	0.17	0.01	71
	5.3	10.62	0.07	0.18	0.01	165
	7.9	27.12	±0.02	0.09	0.01	60
	10.4	8.70	0.09	0.13	0.01	110
NV Aur	-1.2	4.68	-0.10	0.15	0.01	140
	1.7	17.94	-0.06	0.13	0.01	150
	3.0	14.04	-0.04	0.08	0.01	170
R Aur	-7.5	12.48	0.0	0.0	0.01	60
	-5.6	31.56	-0.09	0.27	0.01	90
	-3.7	36.00	-0.13	0.34	0.01	85
	-1.2	38.58	-0.07	0.16	0.01	90
	-0.1	13.14	-0.12	0.27	0.01	90
RU Aur	-38.2	1.85	0.08	0.15	0.02	120
	-34.9	1.05	-0.12	0.40	0.02	85
	-33.2	0.25	-0.22	0.40	0.02	40
	-27.1	0.2	0.0	0.35	0.02	175
TX Cam	5.0	11.52	-0.06	0.16	0.02	130
	6.1	13.68	-0.03	0.08	0.02	80
	8.0	23.46	0.04	0.20	0.01	175
	10.1	117.06	-0.01	0.17	0.01	175
	11.3	26.46	0.03	0.06	0.01	170
	13.2	22.62	-0.03	0.05	0.02	50
	14.9	12.78	0.02	0.18	0.02	185
V Cam	3.8	3.12	-0.04	0.22	0.01	0
	7.6	12.72	0.0	0.04	0.01	160
	9.0	9.24	0.02	0.05	0.01	0
R Cnc	9.2	2.70	0.12	0.26	0.01	100
	10.3	5.16	-0.02	0.04	0.01	160
	13.7	56.46	0.02	0.17	0.01	90
	15.8	33.66	-0.01	0.06	0.01	180
W Cnc	33.9	21.18	0.13	0.32	0.01	40
	41.9	2.82	-0.03	0.12	0.01	150

Table 2. (-continued). Derived parameters of the different components of the SiO maser emission profile for each star. Only the well identified components are given (distinct peak or strong wing emission separated from the bulk emission). Note that the polarization is fractional. The δP is the rms derived from the p_C plot.

Source	v_{LSR} [km s^{-1}]	F_ν [Jy]	p_c	p_L	δp	χ [°]
VY CMa	5.2	553.4	-0.01	0.02	0.05	125
	8.5	973.3	0.0	0.01	0.05	160
	11.3	1086.7	0.04	0.06	0.05	110
	14.9	559.0	-0.02	0.03	0.05	80
	17.6	553.0	-0.03	0.08	0.05	160
	19.5	769.2	0.0	0.0	0.05	160
	22.7	1569.0	-0.04	0.13	0.05	0
	38.7	207.3	-0.01	0.01	0.05	150
S CMi	50.1	3.61	0.07	0.36	0.01	50
	52.1	11.42	0.03	0.16	0.01	50
	54.9	3.89	0.0	0.0	0.02	75
R Cas	25.4	600.0	0.06	0.20	0.01	25
	27.1	780.1	0.03	0.09	0.01	70
	28.4	419.6	-0.02	0.08	0.01	90
S Cas	-32.5	1.38	0.0	0.0	0.01	85
	-30.0	11.52	-0.32	0.52	0.01	110
	-28.3	2.94	0.12	0.17	0.01	20
	-27.2	4.98	0.05	0.05	0.01	20
T Cas	-11.2	1.62	0.11	0.27	0.01	110
	-8.7	11.70	-0.02	0.18	0.01	100
	-5.1	5.82	0.08	0.12	0.01	140
T Cep	-2.5	63.00	±0.03	0.05	0.01	100
	-0.5	117.42	0.04	0.16	0.01	140
	0.8	36.00	-0.04	0.05	0.01	105
R Com	-4.4	7.50	-0.04	0.10	0.01	80
	-3.3	8.82	0.07	0.27	0.01	20
	-1.4	3.42	0.02	0.35	0.01	50
S Crb	0.8	41.40	0.07	0.17	0.01	75
	2.0	64.44	0.0	0.22	0.01	70
	4.9	28.62	0.0	0.35	0.01	160
R Crt	4.5	4.02	-0.07	0.13	0.01	100
	10.4	36.84	0.0	0.0	0.01	50
	16.4	4.74	-0.08	0.15	0.01	120
χ Cyg	7.1	50.16	-0.19	0.42	0.01	75
	10.0	206.1	0.11	0.32	0.01	140
	14.6	36.72	0.0	0.0	0.01	190
UX Cyg	-1.3	9.12	-0.04	0.08	0.01	100
	-0.5	21.96	0.01	0.06	0.01	110
	0.8	44.22	0.02	0.06	0.01	175
R Hya	-11.2	31.14	0.09	0.34	0.01	135
	-10.0	67.08	0.10	0.34	0.01	140
	-8.9	182.82	0.02	0.06	0.01	150
	-6.6	146.22	0.05	0.25	0.01	130
W Hya	37.8	151.20	0.02	0.07	0.005	70
	41.4	934.38	±0.02	0.03	0.005	150
	44.8	202.02	0.06	0.15	0.005	100
X Hya	21.8	4.26	0.01	0.70	0.01	80
	23.6	3.18	0.03	0.25	0.01	60
	28.9	23.28	-0.01	0.08	0.01	170
R Leo	-1.4	195.30	0.10	0.30	0.01	140
	0.5	1110.6	-0.09	0.36	0.01	80

Table 2. (-continued). Derived parameters of the different components of the SiO maser emission profile for each star. Only the well identified components are given (distinct peak or strong wing emission separated from the bulk emission). Note that the polarization is fractional. The δP is the rms derived from the p_C plot.

Source	v_{LSR} [km s^{-1}]	F_ν [Jy]	p_c	p_L	δp	χ [°]
W Leo	42.7	2.04	0.0	0.18	0.05	170
	44.6	2.76	0.0	0.10	0.05	100
	47.9	3.30	0.0	0.20	0.05	170
	54.2	4.62	0.08	0.42	0.02	35
R LMi	0.3	61.98	0.0	0.02	0.01	25
	2.2	52.80	0.12	0.36	0.01	0
	3.5	34. 62	0.06	0.20	0.01	15
	4.5	14.16	0.04	0.08	0.01	20
	6.2	10.56	0.05	0.20	0.01	80
T Lep	-32.0	15.48	-0.11	0.34	0.01	10
	-30.1	10.74	-0.06	0.20	0.01	20
	-27.1	42.48	0.03	0.10	0.01	95
	-25.4	7.80	0.10	0.14	0.01	75
RS Lib	3.2	7.62	0.01	0.08	0.01	150
	6.5	35.94	-0.10	0.15	0.01	150
	9.1	12.24	-0.06	0.20	0.01	150
Ap Lyn	-25.1	9.90	0.02	0.37	0.01	185
	-23.0	36.36	0.12	0.65	0.01	165
	-20.9	9.24	0.03	0.20	0.01	150
U Lyn	-14.0	12.00	-0.02	0.04	0.01	45
	-11.7	30.78	0.0	0.08	0.01	40
	-4.5	7.19	-0.13	0.24	0.01	80
GX Mon	-10.4	29.64	0.12	0.38	0.01	100
	-8.5	21.60	-0.03	0.08	0.01	20
	-6.4	10.38	0.07	0.20	0.01	120
	-4.9	7.92	-0.02	0.07	0.01	160
	-3.0	4.98	0.01	0.02	0.01	55
SY Mon	-59.6	3.01	0.12	0.58	0.02	75
	-56.0	2.52	-0.05	0.15	0.02	30
V Mon	2.0	8.58	0.05	0.10	0.02	170
	4.8	3.12	0.05	0.14	0.02	80
U Ori	-42.4	12.42	0.05	0.15	0.01	80
	-39.9	46.26	-0.04	0.16	0.01	50
	-37.8	13.08	0.02	0.06	0.01	145
	-34.2	32.40	0.13	0.40	0.01	170
RR Per	5.1	10.81	0.03	0.14	0.01	165
	7.5	29.46	0.11	0.43	0.01	175
	8.6	27.78	0.03	0.30	0.01	185
	11.1	13.02	0.10	0.34	0.01	180
S Per	-47.4	7.02	-0.03	0.03	0.02	75
	-44.9	31.62	0.15	0.04	0.05	190
	-43.3	35.70	0.01	0.04	0.05	190
	-39.2	71.16	0.0	0.03	0.05	150
	-36.0	37.79	±0.03	0.06	0.02	80
QX Pup	27.3	11.22	0.02	0.15	0.01	120
	29.4	6.84	0.0	0.03	0.01	70
	35.3	9.12	0.17	0.41	0.01	120
	41.6	2.70	0.04	0.07	0.01	10
Z Pup	3.9	40.98	0.07	0.23	0.01	140
VX Sgr	-6.1	25.98	0.0	0.0	0.005	140
	0.9	89.16	0.01	0.02	0.005	130
	3.4	122.39	-0.02	0.05	0.005	10
	5.7	178.38	-0.01	0.04	0.005	10
	10.1	114.61	-0.03	0.10	0.005	145
	14.1	53.34	0.01	0.01	0.005	145
	16.2	80.04	0.01	0.02	0.005	160

Table 2. (-continued). Derived parameters of the different components of the SiO maser emission profile for each star. Only the well identified components are given (distinct peak or strong wing emission separated from the bulk emission). Note that the polarization is fractional. The δP is the rms derived from the p_C plot.

Source	v_{LSR} [km s^{-1}]	F_ν [Jy]	p_c	p_L	δp	χ [°]
AH Sco	-11.4	26.69	0.05	0.06	0.005	120
	-10.0	48.31	0.01	0.02	0.005	120
	-7.2	78.78	0.0	0.0	0.005	150
	-4.7	54.74	0.0	0.02	0.005	20
	-2.8	32.99	-0.02	0.05	0.005	170
RR Sco	-33.9	4.02	0.10	0.14	0.02	65
	-30.2	9.48	0.0	±0.07	0.02	85
	-26.5	11.16	0.04	0.10	0.02	90
	-23.2	2.82	0.06	0.16	0.02	55
R Ser	27.8	21.61	-0.07	0.30	0.01	40
S Ser	18.7	11.22	0.04	0.09	0.01	180
	20.9	16.92	0.0	0.06	0.01	100
WX Ser	4.1	20.34	-0.05	0.15	0.01	140
	6.6	12.18	0.04	0.15	0.01	80
	9.8	8.41	-0.12	0.30	0.01	140
IK Tau	31.6	46.74	0.04	0.14	0.01	180
	34.7	288.24	0.05	0.16	0.01	170
	36.8	53.04	0.07	0.18	0.01	140
	39.6	27.84	0.13	0.36	0.01	125
R Tau	9.5	3.78	-0.10	0.15	0.01	60
	11.8	19.51	0.06	0.13	0.01	150
	13.1	10.26	0.07	0.19	0.01	140
	14.7	7.68	-0.09	0.31	0.01	55
	16.4	6.24	-0.08	0.19	0.01	75
	19.0	3.24	-0.20	0.44	0.01	55
RX Tau	-44.0	3.36	-0.06	0.10	0.02	120
	-41.0	10.98	-0.01	0.01	0.02	100
	-38.9	2.94	0.04	0.15	0.02	170
R Tri	56.7	13.62	-0.05	0.24	0.01	105
R UMi	-6.1	1.98	0.0	0.25	0.05	110
S UMi	-44.4	21.54	0.0	0.0	0.005	30
	-43.3	30.66	0.0	0.01	0.005	20
	-40.8	24.24	-0.02	0.10	0.005	10
	-40.0	27.66	0.02	0.07	0.005	10
R Vir	-26.8	0.84	0.15	0.30	0.05	170
	-25.7	2.16	-0.10	0.15	0.02	10
RS Vir	-15.7	2.64	-0.11	0.18	0.01	0
	-13.3	10.62	-0.08	0.32	0.01	150
	-12.5	8.46	0.0	0.20	0.01	0
	-9.1	7.08	-0.06	0.52	0.01	160
RT Vir	9.1	1.20	0.0	0.02	0.02	70
	13.8	2.22	0.12	0.19	0.02	20
	15.7	3.12	0.12	0.20	0.02	140
	18.0	7.98	0.0	0.06	0.02	130
	20.7	3.48	-0.10	0.12	0.02	120
	22.6	3.03	-0.06	0.11	0.02	60
	27.7	2.34	-0.04	0.10	0.02	40
S Vir	10.3	13.62	-0.04	0.27	0.01	180
	12.2	7.79	0.03	0.06	0.01	105
	13.7	22.52	-0.05	0.19	0.01	130

Table 3. Average magnetic field strengths derived from p_C.

Source	$B_{//}$ (G)
IRAS18055-1433	4.6-13.9
IRAS18158-1527	3.7-20.0
IRAS18204-1344	0-3.2
W And	0.4-5.9
AU Aur	0.9-4.2
NV Aur	1.9-4.6
R Aur	0-6.0
RU Aur	0-10.2
TX Cam	0.4-2.8
V Cam	0-1.9
R Cnc	0.4-5.6
W Cnc	1.4-6.0
VY CMa	0-1.9
S CMi	0-3.2
R Cas	0.9-2.8
S Cas	0-14.9
T Cas	0.9-5.1
T Cep	1.4-1.9
R Com	0.9-3.2
S Crb	0-3.2
R Crt	0-3.7
χ Cyg	0-8.8
UX Cyg	0.4-1.9
R Hya	0.9-4.6
W Hya	0.9-2.8
X Hya	0.4-1.4
R Leo	4.2-4.6
W Leo	0-3.7
R LMi	0-5.6
T Lep	1.4-5.1
RS Lib	0.4-4.6
Ap Lyn	0.9-5.6
U Lyn	0-6.0
GX Mon	0.4-5.6
SY Mon	2.3-5.6
V Mon	2.3
U Ori	0.9-6.0
RR Per	1.4-5.1
S Per	0-7.0
QX Pup	0-7.9
Z Pup	3.2
VX Sgr	0-1.4
AH Sco	0-2.3
RR Sco	0-4.6
R Ser	3.2
S Ser	0-1.9
WX Ser	1.9-5.6
IK Tau	1.9-6.0
R Tau	2.8-9.3
RX Tau	0.4-2.8
R Tri	2.3
R UMi	0
S UMi	0-0.9
R Vir	4.6-7.0
RS Vir	0-5.1
RT Vir	0-5.6
S Vir	1.4-2.3

Online Material

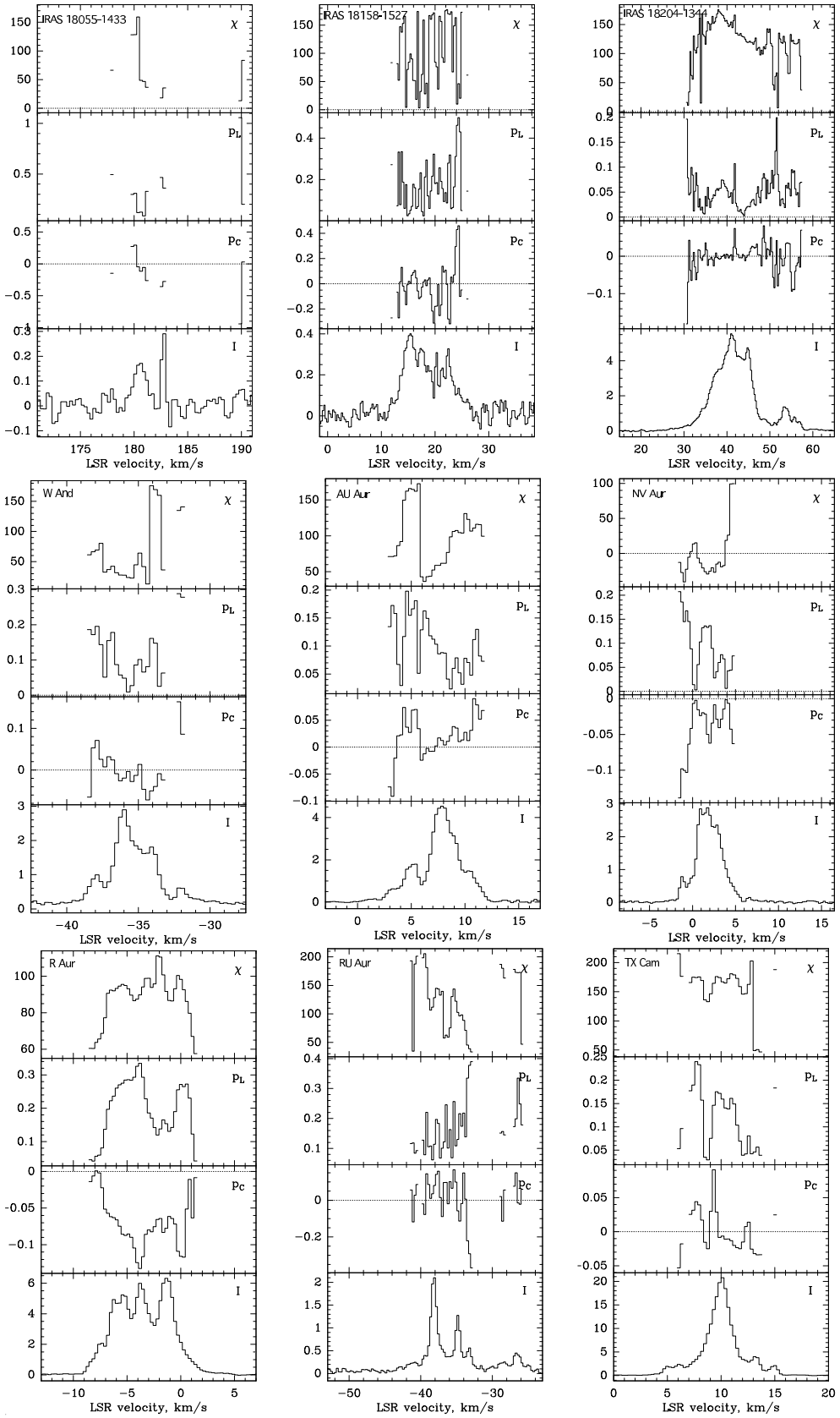


Fig. 2. Position angle of polarization (χ) in degrees, linear (p_L) and circular (p_C) polarization levels and intensity ($I = Ta^{\star}$ in Kelvin; the conversion factor is 6 Jy/K) for the SiO emission observed in several stars.

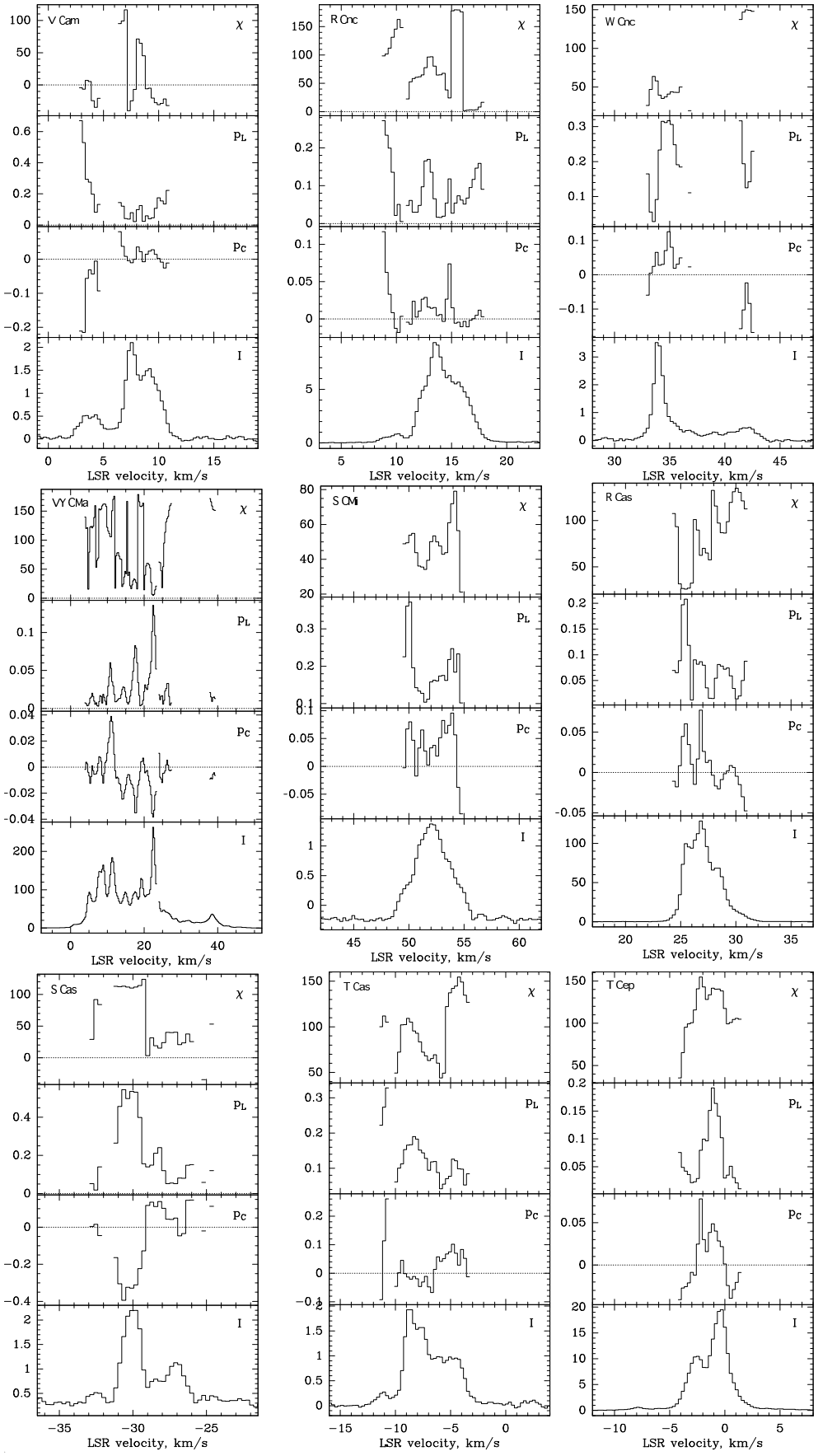


Fig. 2. (-continued). Position angle of polarization (χ) in degrees, linear (p_L) and circular (p_C) polarization levels and intensity ($I = Ta^\star$ in Kelvin; the conversion factor is 6 Jy/K) for the SiO emission observed in several stars.

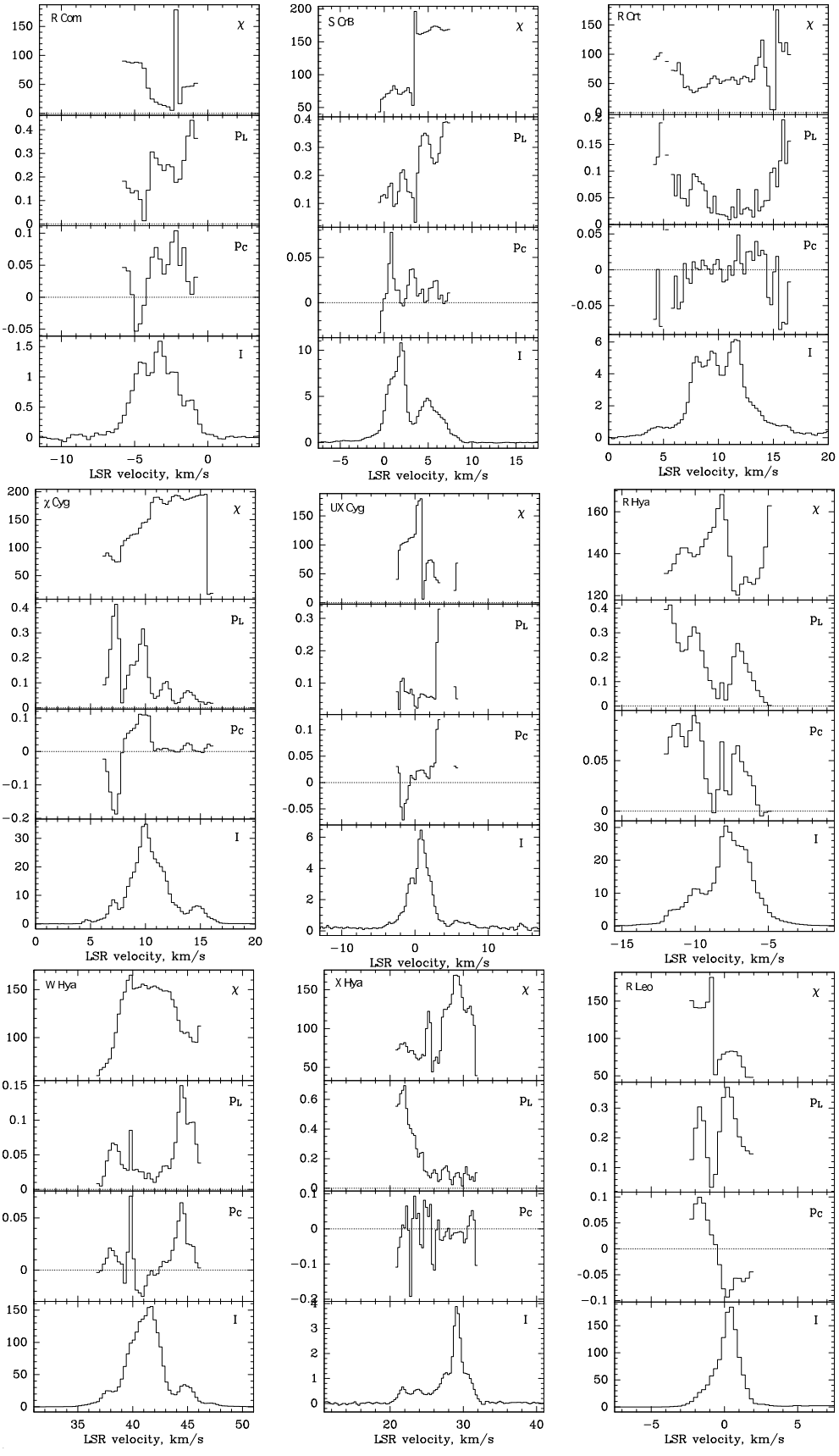


Fig. 2. (-continued). Position angle of polarization (χ) in degrees, linear (p_L) and circular (p_C) polarization levels and intensity ($I = Ta^{\star}$ in Kelvin; the conversion factor is 6 Jy/K) for the SiO emission observed in several stars.

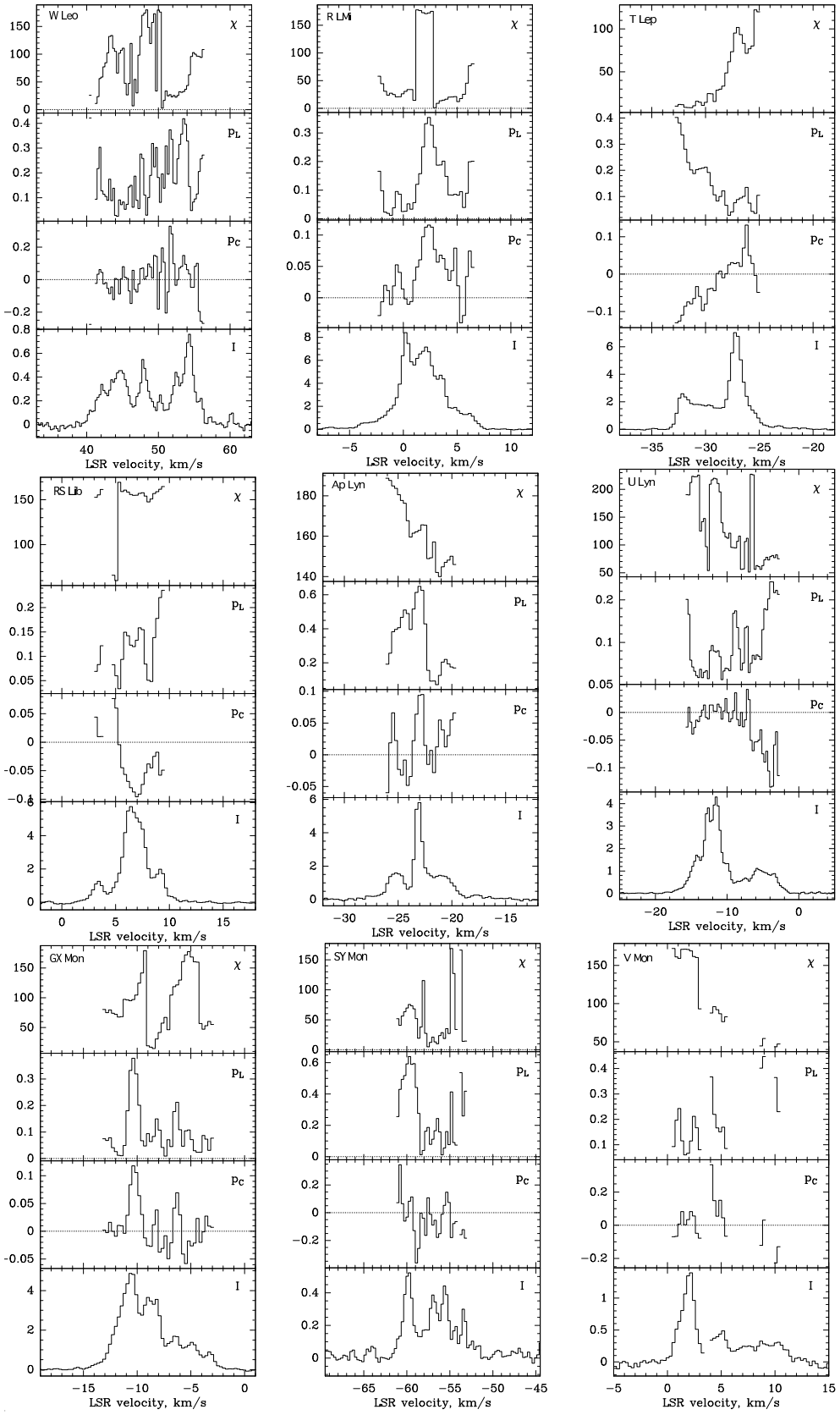


Fig. 2. (-continued). Position angle of polarization (χ) in degrees, linear (p_L) and circular (p_C) polarization levels and intensity ($I = Ta^{\star}$ in Kelvin; the conversion factor is 6 Jy/K) for the SiO emission observed in several stars.

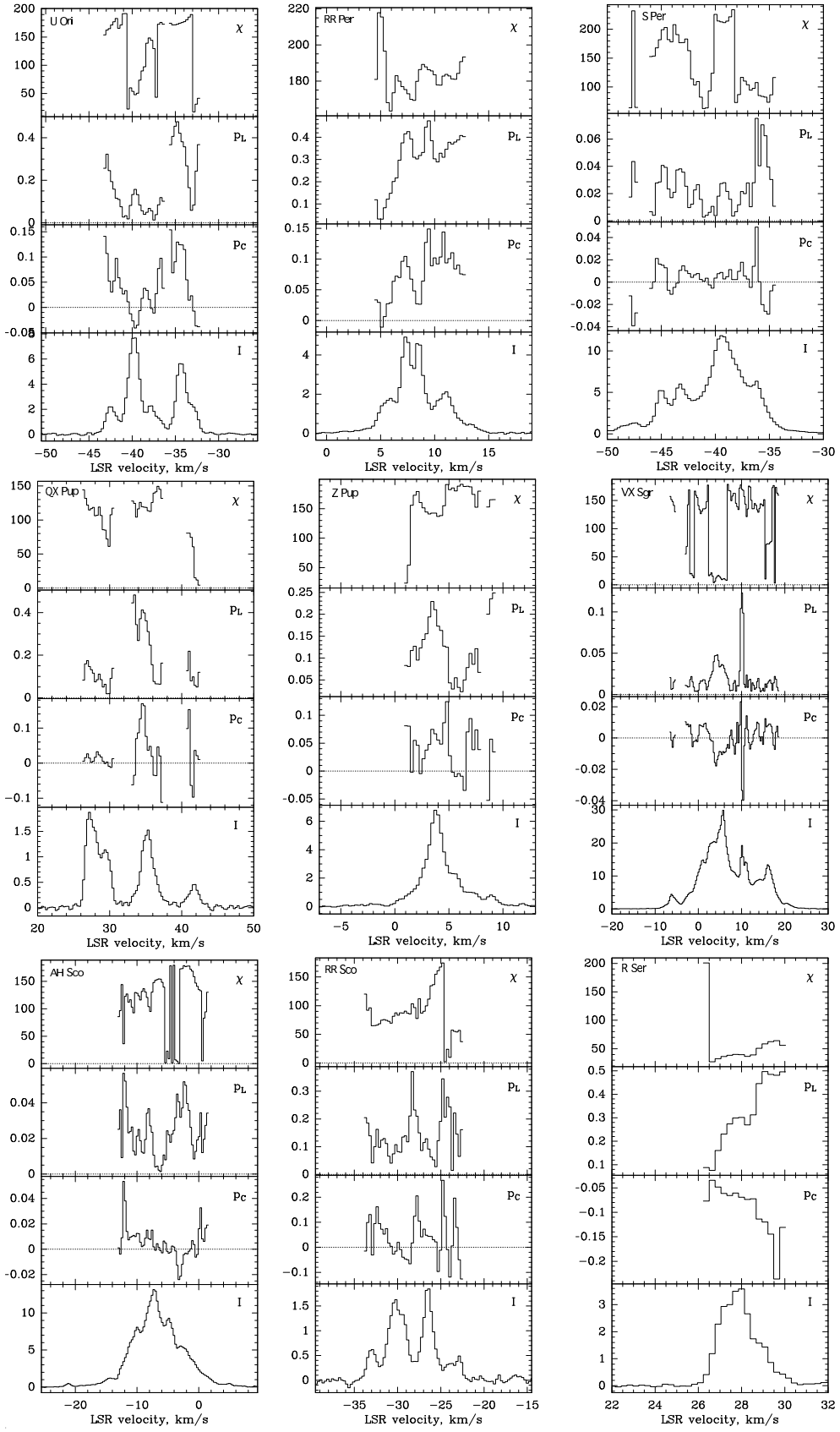


Fig. 2. (-continued). Position angle of polarization (χ) in degrees, linear (p_L) and circular (p_C) polarization levels and intensity ($I = Ta^{\star}$ in Kelvin; the conversion factor is 6 Jy/K) for the SiO emission observed in several stars.

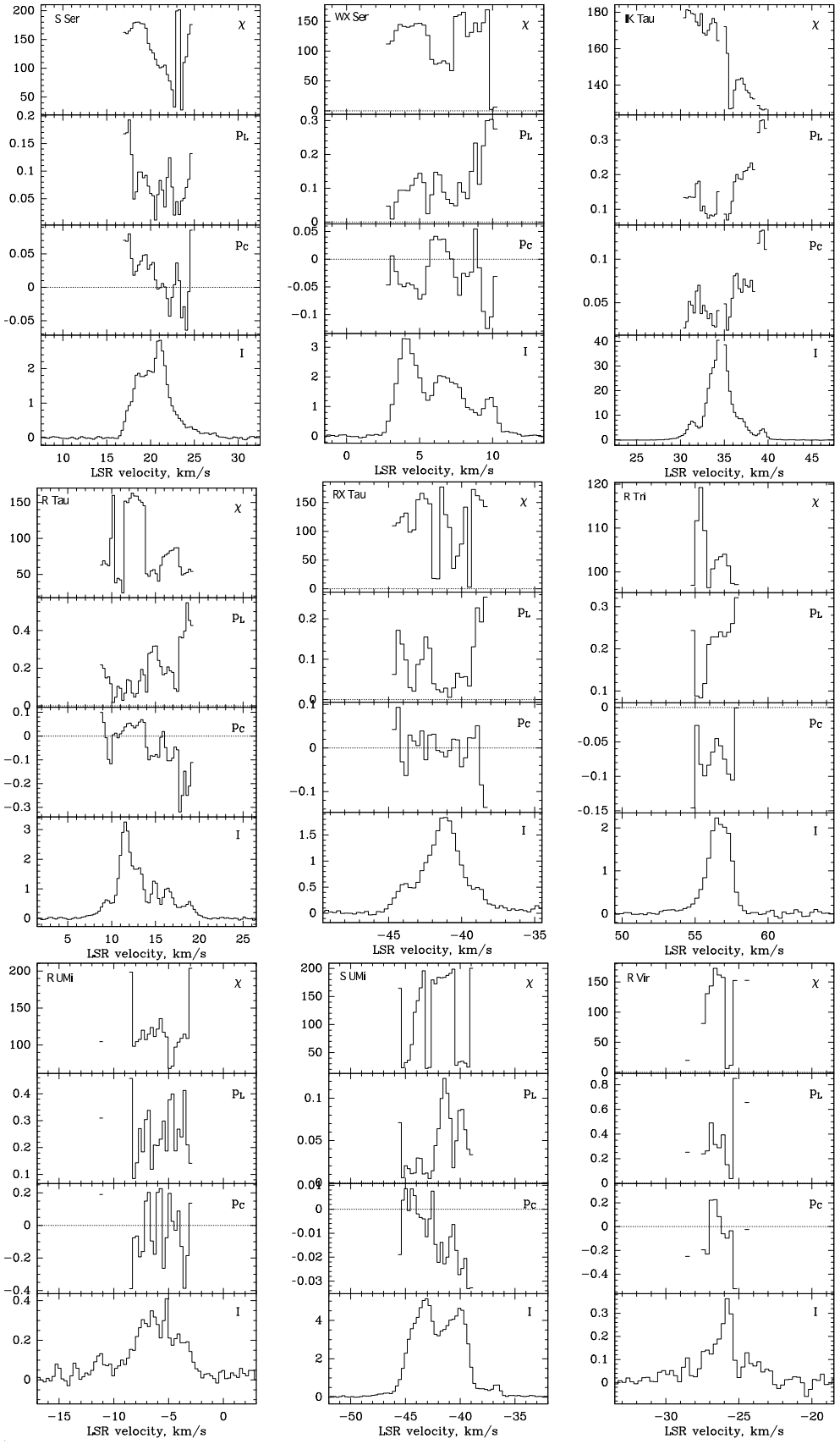


Fig. 2. (-continued). Position angle of polarization (χ) in degrees, linear (p_L) and circular (p_C) polarization levels and intensity ($I = Ta^{\star}$ in Kelvin; the conversion factor is 6 Jy/K) for the SiO emission observed in several stars.

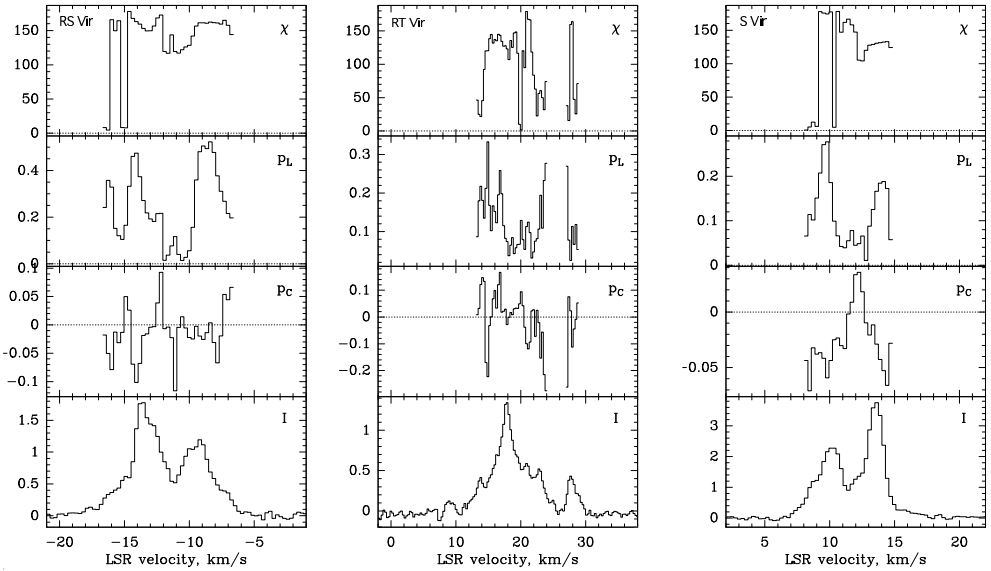


Fig. 2. (-continued). Position angle of polarization (χ) in degrees, linear (p_L) and circular (p_C) polarization levels and intensity ($I = Ta^\star$ in Kelvin; the conversion factor is 6 Jy/K) for the SiO emission observed in several stars.